mTOR Inhibitor RAD001 (Everolimus) Has Antiangiogenic/Vascular Properties Distinct from a VEGFR Tyrosine Kinase Inhibitor

Heidi A. Lane,[2] Jeanette M. Wood,[3] Paul M.J. McSheehy,[1] Peter R. Allegrini,[1] Anne Boulay,[1] Joseph Brueggen,[1] Amanda Littlewood-Evans,[1] Sauveur-Michel Maira,[1] Georg Martiny-Baron,[1] Christian R. Schnell,[1] Patrizia Sini,[4] and Terence O'Reilly[1]

Abstract

Purpose: Comparison of the antiangiogenic/vascular properties of the oral mammalian target of rapamycin (mTOR) inhibitor RAD001 (everolimus) and the vascular endothelial growth factor receptor (VEGFR) inhibitor vatalanib (PTK/ZK).

Experimental Design: Antiproliferative activity against various tumor histotypes and downstream effects on the mTOR pathway were measured *in vitro*. *In vivo*, antitumor activity, plasma, and tumor RAD001 levels were measured. Activity in several different angiogenic/vascular assays *in vitro* and *in vivo* was assessed and compared with PTK/ZK.

Results: RAD001 inhibited proliferation *in vitro* (IC_{50} values <1 nmol/L to >1 μmol/L), and in sensitive and insensitive tumor cells, pS6 kinase and 4E-BP1 were inhibited. Activity *in vitro* did not correlate with activity *in vivo* and significant responses were seen in tumors with IC_{50} values >10-fold higher than tumor RAD001 concentrations. *In vitro*, RAD001 inhibited the proliferation of VEGF-stimulated and fibroblast growth factor-stimulated human endothelial cells but not dermal fibroblasts and impaired VEGF release from both sensitive and insensitive tumor cells but did not inhibit migration of human endothelial cells. *In vivo*, in tumor models derived from either sensitive or insensitive cells, RAD001 reduced Tie-2 levels, the amount of mature and immature vessels, total plasma, and tumor VEGF. RAD001 did not affect blood vessel leakiness in normal vasculature acutely exposed to VEGF nor did it affect tumor vascular permeability (K^{trans}) as measured by dynamic contrast-enhanced magnetic resonance imaging. However, the pan-VEGFR inhibitor PTK/ZK inhibited endothelial cell migration and vascular permeability but had less effect on mature vessels compared with RAD001.

Conclusions: VEGFR and mTOR inhibitors show similar but also distinct effects on tumor vascular biology, which has implications for their clinical activity alone or in combination.

RAD001 (everolimus) is an orally active derivative of rapamycin currently in phase II/III clinical trials for its utility, alone and in combination, as an anticancer agent. The target of this class of agents is mammalian target of rapamycin (mTOR), a multifunctional signal transducing protein, which obtains signals from many upstream pathways including nutrient supply and propagates the information via regulation of multiple downstream pathways (1–3). Rapamycins function to block mTOR activity by binding to the immunophilin FKBP-12, which forms an inhibitory complex that binds with high affinity to mTOR in the rapamycin-sensitive mTOR-RAPTOR complex (4, 5). However, a rapamycin-insensitive pathway also exists when mTOR is complexed with RICTOR (6). Besides serving a key role in normal cell physiology, mTOR has been implicated in cancer; consequently, inhibition of this target has received considerable attention as an anticancer approach (1, 5), leading to the clinical development of rapamycin analogues with improved drug-like properties such as RAD001.

Most solid tumors, regardless of their type and origin, cannot grow beyond a certain size (~1 mm^3) until they establish a blood supply by inducing the formation of new vessels sprouting from existing host capillaries, a process known as angiogenesis (7). Accumulating evidence suggests mTOR to be a critical component of this process (8), because it is part of the phosphatidylinositol 3-kinase/Akt/mTOR signaling pathway, which is also implicated in tumor angiogenesis (9). Although the importance of mTOR signaling in the deregulated cell growth characteristics of human tumor cells is now widely accepted (2, 4, 5), this pathway is also emerging as a key regulator of hypoxia and growth factor-mediated expression of tumor hypoxia-inducible factor-1α (HIF-1α) and HIF-1α-responsive genes, such as vascular endothelial growth factor

Authors' Affiliations: [1]Oncology Research, Novartis Institutes for Biomedical Research; [2]Basilea Pharmaceutica International AG, Basel, Switzerland; [3]S*BIO Pte Ltd, Singapore, Singapore; and [4]Cancer and Infection Research Area, AstraZeneca Pharmaceuticals, Macclesfield, United Kingdom

Received 8/6/08; revised 11/7/08; accepted 11/11/08; published OnlineFirst 02/17/2009.

The costs of publication of this article were defrayed in part by the payment of page charges. This article must therefore be hereby marked *advertisement* in accordance with 18 U.S.C. Section 1734 solely to indicate this fact.

Note: Supplementary data for this article are available at Clinical Cancer Research Online (http://clincancerres.aacrjournals.org/).

H.A. Lane and J.M. Wood contributed equally to this work.

Requests for reprints: Paul McSheehy, Oncology Research, Novartis Pharma AG, WKL-125.13.17, Basel CH-4002, Switzerland. Phone: 41-61-696-8189; E-mail: paul_mj.mcsheehy@novartis.com.

doi:10.1158/1078-0432.CCR-08-2057

Translational Relevance

Data show a broad antiproliferative activity of the novel mammalian target of rapamycin inhibitor RAD001 (everolimus) on tumor cell lines *in vitro*, with some cells being very sensitive (IC_{50} < 1 nmol/L) and others essentially insensitive (IC_{50} > 1 μmol/L). However, activity *in vitro* did not predict activity *in vivo*, where activity was seen despite tumor levels of the compound being >10-fold below the IC_{50} in some models. These data suggested an antiangiogenic and/or antivascular activity of RAD001. Antiangiogenic and antivascular properties were studied using various models *in vitro* and *in vivo* and were compared with the pan-vascular endothelial growth factor receptor (VEGFR) inhibitor vatalanib (PTK/ZK), which showed similar but also dissimilar activity in the same models. Thus, clinical anticancer activity of RAD001 may include effects directed at both tumor and stroma of solid tumors with a mechanism of action distinct from agents targeting the VEGFR signaling pathway. This suggests that RAD001 should have broad activity as a monotherapy and furthermore may be of value pretreatment and post-treatment with VEGFR inhibitors as well as in combination with such agents.

(VEGF), as well as endothelial cell function and other stromal cells, thereby regulating tumor vascularization (10–12). Furthermore, mTOR is considered to be very well conserved and ubiquitously expressed including also in endothelial cells (13).

RAD001 has been shown previously to have antiangiogenic effects including inhibition of human umbilical vein endothelial cell (HUVEC) growth *in vitro*, reductions in expression of HIF-1 and VEGF in cultured tumor cells (14–17), and reductions in blood vessel density (BVD) in several different experimental tumor models (15–17). Similar observations are reported for rapamycin (18–20) and the rapamycin prodrug temsirolimus (21, 22). The studies we report here expand on this information by comparing the antiangiogenic and antivascular effects caused by mTOR pathway inhibition by RAD001 with those of the pan-VEGF receptor (VEGFR) inhibitor vatalanib (PTK/ZK). We show that RAD001 has significant antitumor activity in mouse tumor models irrespective of *in vitro* sensitivity of the tumor cell lines used or apparently inadequate drug exposure in tumor tissue for antiproliferative activity in the insensitive models. Moreover, in both scenarios, a marked reduction in tumor vascularization and plasma VEGF production is observed. Comparisons of the effects of RAD001 on angiogenic processes both *in vitro* and *in vivo* with those of PTK/ZK indicate overlapping effects on some aspects of endothelial cell biology and angiogenic processes, confirming an integral role of the mTOR pathway in VEGFR-induced proliferative pathways. However, some important distinctions exist between the effects of a mTOR inhibitor as opposed to a VEGFR inhibitor, which have implications for their application in the clinic as monotherapies or in their combination.

Materials and Methods

Compounds and cells. RAD001 and PTK/ZK were synthesized at Novartis Institutes for Biomedical Research and Bayer-Schering Pharma. Stock solutions of RAD001 and PTK/ZK for enzyme or cellular assays were prepared from dry substance in DMSO and then diluted in the optimal medium. The final concentration of DMSO in any incubation mixture did not exceed 0.1% (v/v). For all *in vivo* experiments, a microemulsion of RAD001 was freshly diluted in a vehicle of 5% glucose (administration volume 10 mL/kg, freshly thawed). PTK/ZK was administered in a vehicle of 100% PEG-300 (dose volume 5 mL/kg).

Unless indicated otherwise, chemicals were obtained from Fluka Chemie.

The following human tumor cell lines were obtained from the American Type Culture Collection: colon HCT-116; lung A549, NCI-H520, and NCI-H596; renal Caki-1 and 786-O; glioma U87MG and BS153; breast MDA-MB-231 and BT474; and melanoma A375 and A2058. Human cervical carcinoma KB-31 and KB-8511 cells were obtained from Dr. R.M. Baker (RPMI). The murine melanoma cell line B16/BL6 was obtained from Dr. I.J. Fidler (M. D. Anderson Cancer Center) and the murine fibrosarcoma cell line RIF-1 was obtained from L. Rodrigues (St. George's Hospital Medical School). The rat pituitary cell line GH3 was obtained from the European cell culture collection, whereas a cell line for BN472 rat mammary tumors is not available (see below). HUVEC and normal human dermal fibroblasts were obtained from Promo Cell (BioConcept). Cells were maintained and cultured according to established techniques at 37°C in 5% (v/v) CO_2 at 80% relative humidity using culture medium recommended by the supplier. Cell culture media and additives were obtained from Life Technologies or AMIMED.

Ligands and antibodies. Purified human VEGF and human soluble Tie-2Fc were produced in-house and the capture Tie-2 antibody was obtained from Upstate (mAb33). Human basic fibroblast growth factor (bFGF) was obtained from Life Technologies (product 13256-029). The human and mouse VEGF ELISAs and the Tie-2 detection antibody (AF762) were obtained from R&D Systems. Rat anti-mouse CD31 was obtained from Pharmingen (clone Mec 13.3). The rabbit anti-mouse smooth muscle actin (SMA)-Cy3 conjugate (clone 1A4) and the alkaline phosphatase-conjugated goat anti-rabbit IgG (A-8062) were obtained from Sigma. The Alexa Fluor 568-conjugated goat anti-rat secondary antibody was obtained from Molecular Probes.

Cell proliferation and migration assays. Tumor cells were plated into 96-well plates at densities ranging from 500 to 5,000/100 μL/well, with repeat experiments being done at an optimal cell number, typically 1,000 to 2,000 per well, and incubated overnight. Cells were exposed to RAD001 and incubated for 4 days and the cell number was determined by methylene blue staining. For this, 50 μL glutaraldehyde [20% (v/v)] was added to the wells incubated for 10 min at room temperature. The culture medium was aspirated, cells were washed with distilled water, and 100 μL methylene blue [0.05% (w/v) in water] was added and incubated for 10 min at 37°C. Stained cells were washed three times with water, 200 μL HCl [3% (v/v)] was added, and the plate shaken at room temperature for 20 min. The absorbance of each well was determined at 650 nm. The IC_{50} values (the concentration of compound to reduce the methlyene blue staining by 50% of controls) were calculated using Softmax 2.0 software.

The effects of RAD001 on serum-, VEGF-, or bFGF-induced HUVEC proliferation were tested using a proliferation assay based on bromodeoxyuridine incorporation (Biotrak Cell Proliferation ELISA System version 2; Amersham) as described previously (23). As a control, effects on bFGF-induced proliferation of normal human dermal fibroblasts were also determined. The effects of RAD001 on VEGF-induced migration of HUVEC were tested using a Boyden chamber method as described previously (23).

In vivo *growth factor-induced angiogenesis model.* VEGF-mediated angiogenesis *in vivo* was induced in a growth factor implant model in mice as described previously (23). We have shown that VEGF induces dose-dependent increases in weight, hemoglobin (converted to equivalents of blood), and Tie-2 content (number of endothelial cells and therefore vessel density) of the adherent, vascularized tissue

growing around the chambers and that this response is blocked by antibodies that specifically neutralize VEGF or by VEGFR tyrosine kinase inhibitors.

Measurement of Tie-2 concentrations in the angiogenesis implant model and tumors. Nunc Maxsisorb 96-well plates were coated overnight at 4°C with 0.1 mL anti-Tie-2 AB33 at the concentrations indicated (standard concentration, 2 μg/mL). Wells were washed three times with 0.2 mL TPBS, blocked by shaking with 3% Top-Block for 2 h, and washed three times with TPBS and protein lysates (0.1-5 mg in a total volume of 0.2 mL) were added for 2 h. Recombinant human soluble Tie-2Fc dissolved in radioimmunoprecipitation assay buffer was used as standard in a concentration range from 0.1 to 300 ng/well. After washing, detection antibody (50 μL antibody solution at 1 μg/mL and an alkaline phosphatase-conjugated anti-goat monoclonal, 50 μL in a dilution of 1:3,000) in PBS-Tween 20 + 0.1% Top-Block was applied for 1 h at room temperature. After washing three times with TPBS, Tie-2 antibody complexes were detected by incubating with *p*-nitrophenyl-phosphate (Sigma) and reading absorbance with an ELISA reader at 405 nm. Quantification of Tie-2 was done by plotting the absorbance against log soluble Tie-2-Fc concentration from the standard curve. Data were analyzed with GraphPad Prism (GraphPad Software), fitting a sigmoidal response curve: Y = bottom + (top - bottom) / $(1 + 10^{(\log EC50 - X)})$.

***Measurement of VEGF-induced vascular leakiness* in vivo.** Heparin immobilized on acrylic beads (50-100 μm radius; Sigma) were incubated overnight at 4°C with either PBS (control side) or human $VEGF_{165}$ (~1.3 ng/bead; opposite side) and subsequently were implanted subcutaneously in both ears of each mouse (8-10 beads per ear) under isoflurane anesthesia. VEGF induces leakiness of vessels around the beads. Vascular permeability of the newly formed vessels was visualized after 2 days using Evans blue dye (2%, 10 mL/kg), which was injected intravenously 30 min before sacrificing the mice. Measurements of the dye extravasation area (mm^2) were made using computer-assisted image analysis software (KS-400 3.0 imaging system; Zeiss).

In vivo *tumor models: human tumor xenografts, rat GH3 prolactinoma, BN472 mammary, and murine B16/BL6 melanoma.* Healthy pathogen-free female BALB/c *nu/nu* athymic mice were obtained from Iffa Crédo and used for the xenograft experiments, except where Harlan athymic mice were used, which were obtained from Laboratory Animal Services, Novartis Institutes for Biomedical Research. *In vivo* experiments involving B16/BL6 melanoma cells used syngeneic, female, C57BL/6 mice obtained from Iffa Crédo animal breeding facility. *In vivo* experiments using rat GH3 pituitary tumors or BN472 mammary tumors used Wistar-Furth rats or Brown-Norway rats, respectively, which were obtained from Charles River.

All experimental approaches involving animals were approved by the Basel Veterinäramt and all animals had free access to food and water at all times. Athymic mice were kept in a pathogen-controlled environment.

Tumor cells were grown to ~80% confluency and trypsinized, and cell viability was assessed by trypan blue exclusion; only suspensions with >90% viability were used. Cells were resuspended in Hanks' buffer containing 10% (v/v) fetal bovine serum (FBS) and injected subcutaneously in the flank of Wistar rats (GH3 cells), athymic BALB/c, or Harlan athymic mice, except for B16/BL6 cells, which were injected in the ears of C57/BL6 mice as described previously (24). There is no available cell line for BN472 tumors, so these tumors were established by passage of tumor fragments as described previously (25). Human tumors were established by subcutaneous injection in carrier female mice. The resulting tumors were passaged and experiments began on the second passage. Tumor fragments (~25 mg) were implanted subcutaneously into the left flank of mice anesthetized with Forene (3% isoflurane in medical O_2; Abbott). Treatments were initiated when the mean tumor volume reached ~100 mm^3. Tumor volumes were determined according to the formula: length × $(\text{diameter})^2 \times \pi / 6$, where length is the longest dimension and diameter is the shortest dimension. For the B16/BL6 melanoma model, measurements of primary tumor area (mm^2) were carried out under a microscope using computer-assisted image analysis software (KS-400 3.0 imaging system; Zeiss). At the end of the experiments, the animals were sacrificed by exposure to an atmosphere highly enriched with CO_2, cervical lymph nodes were weighed, and the number of lung metastases was counted macroscopically.

RAD001, PTK/ZK, and their respective vehicles were prepared each day just before administration to animals and the administration volume was individually adjusted based on animal body weight. In mice, RAD001 was administered at doses ranging from 0.1 to 10 mg/kg/d orally (10 mL/kg) and predominantly at 2.5 to 10 mg/kg because these doses provided the maximum effect. PTK/ZK was administered at 50 to 100 mg/kg/d orally as described previously (24, 26). In the two rat models, RAD001 was administered three times per week.

Tumor histology. In some experiments, the endothelium of perfused vessels in the tumors was visualized using the nuclear staining dye H33342 (Sigma) by injecting 20 mg/kg in normal saline (10 mg/mL) in the lateral tail vein 1 min before sacrificing the mice. Tumors were excised and snap-frozen in OCT embedding compound in chilled (-70°C) *n*-hexane in a dry ice bath. Cryosections of 10 μm were collected on a Superfrost Plus microscope slide, postfixed in 4% paraformaldehyde in PBS for 5 min at room temperature, washed three times for 5 min in PBS, air dried, and stored at -80°C. Several sections of different regions of the tumor were collected and a representative section from the Hoechst staining for each tumor was chosen for quantification. The whole section was photographed using an imaging system with a program for documenting the number of vessels and their diameter and area of the tumor section. The results are expressed as number of vessels per square millimeter of tumor.

Immunohistochemistry was done in a humidified box to prevent evaporation. Sections of tumors were rehydrated in PBS for 5 min, blocked for 30 min with 10% normal goat serum in PBS containing 0.1% Triton X-100, and incubated for 2 h at room temperature with the primary antibodies rat anti-mouse CD31 (1:600) or mouse anti-mouse SMA-FITC conjugated (1:200) in 3% normal goat serum and 0.1% Triton X-100 in PBS. Sections were washed three times for 5 min with PBS. An Alexa Fluor 568-conjugated goat anti-rat secondary antibody diluted 1:400 in PBS containing 3% normal goat serum and 0.1% Triton X-100 was incubated for 1 h at room temperature before sections were washed three times for 5 min in PBS and slides were mounted. Images were collected with a Nikon Cool-Pix camera. The percentage of $CD31^+$ cells covered with SMA was estimated from the photographs and subdivided into three groups of no coverage at all, partial coverage, and complete coverage.

Measurement of VEGF production. B16/BL6 or KB-31 cells (10^4 per well) were plated in 100 μL medium into 96-well plates for 24 h and then treated with increasing concentrations of RAD001 in medium containing 10% FBS (growing cells) or 0.5% FBS (nongrowing cells) for 24 h. Quantification of the level of VEGF (human for KB-31 and mouse for B16/BL6 tumors) in the supernatants was done by ELISA (Quantikine ELISA kit; R&D Systems). Simultaneous quantification of the number of viable cells (CellTiter 96 AQueous One Solution Cell Proliferation Assay; Promega) was done to allow correction of VEGF levels for cell number.

Plasma and samples were collected in separation tubes, allowed to stand at room temperature for 90 s, and then spun at 4°C for 7 min at 7,000 rpm (Sigma). Whole tumors were excised, flash frozen in liquid nitrogen, and stored at -80°C. Subsequently, tumors were taken up in 500 μL PBS containing 0.1% bovine serum albumin, homogenized (BIO 101, Fastprep, speed: 6.0, time: 2 × 40 s), and centrifuged (Sigma; 4°C, highest speed for 5 min). The VEGF concentration (human for KB-31 and mouse for both KB-31 and B16/BL6 tumors) in the resulting supernatants were measured using ELISA assay kits for murine VEGF (Quantikine ELISA kit; R&D Systems) or human VEGF (R&D Systems).

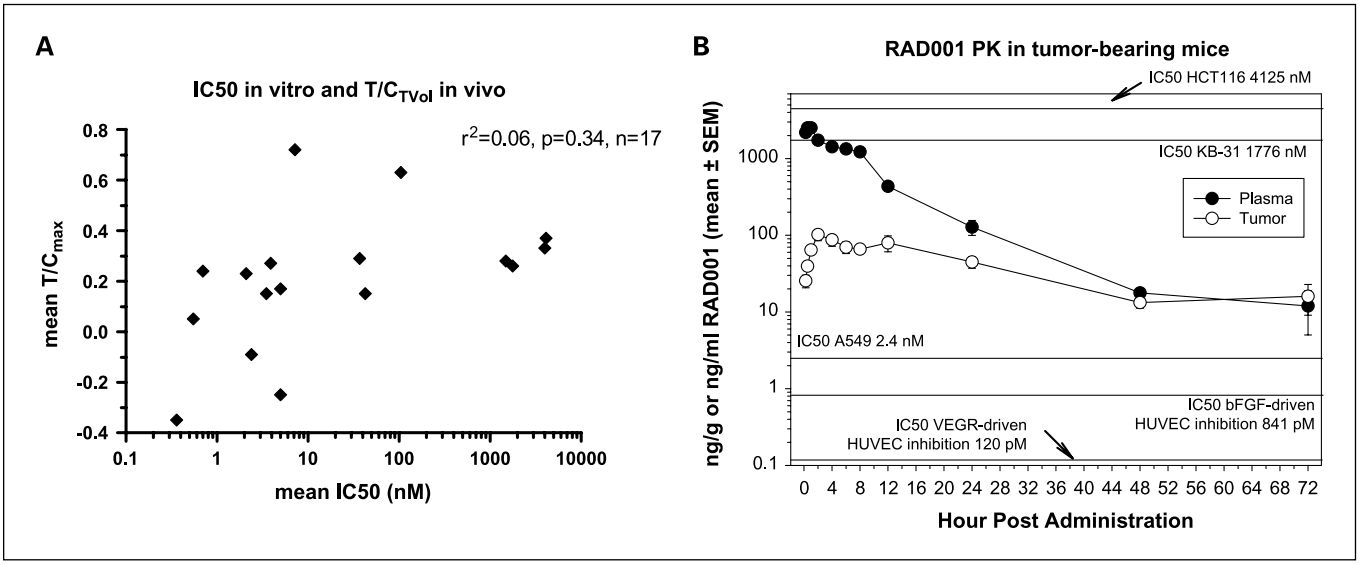

Fig. 1. RAD001 antiproliferative activity and pharmacokinetics. Antiproliferative activity *in vitro* was determined as the IC_{50} on cultured cells and efficacy *in vivo* as the T/C_{TVol} as described in Materials and Methods. Levels of RAD001 in plasma and tumor were determined in tumor-bearing athymic nude mice as described in Materials and Methods. The tumor models used in *A* (n = 17) are identified as follows in order of increasing IC_{50}: renal 786-O, breast BT474, melanoma B16/BL6, pituitary GH3, fibrosarcoma RIF-1, lung A549, glioma BS153, lung H596, glioma U87, breast MDA-MB-231, melanoma A2058, lung H-520, melanoma A375, cervical KB-8511 and KB-31, renal Caki-1, and colon HCT-116.

Determination of RAD001 drug levels in plasma and tumors. Tumor-bearing (tumor volume ~300 mm^3) mice were treated with a single oral administration of 5 mg/kg RAD001. At the allotted times, blood samples were withdrawn into syringes containing EDTA [~0.5% (w/v) final] and plasma was prepared by centrifugation (10,000 × *g*, 5 min). Tumors were excised, weighed, frozen, and stored at -80°C. The determination of RAD001 levels in tumor and plasma was based on a method used for determining the whole blood levels. Briefly, thawed samples were spiked with an internal standard and extracted with *t*-butylmethyl ether, the resultant dried residue was resuspended in aqueous medium, and the analytes were separated and quantitated by high-performance liquid chromatography/mass spectrometry.

Dynamic contrast-enhanced magnetic resonance imaging. For these experiments, animals were divided into two equal groups based on body weight and treated either with vehicle or RAD001 (10 mg/kg/d orally in mice and 5 mg/kg three times per week orally in rats). Directly after the first measurement at baseline (day 0), RAD001 or vehicle was administered orally by gavage (10 mL/kg) for up to 7 days maximum with subsequent magnetic resonance measurements made within 30 min of the last dose.

Mice were anesthetized using 1.5% isoflurane (Abbott) in a 1:2 mixture of O_2/N_2O and placed on an electrically warmed pad for cannulation of one of the two tail veins using a 30-guage needle attached to an infusion line of 30 cm and volume of 80 μL to permit remote administration of the contrast agent. The animals were positioned on a cradle in a supine position inside the 30 cm horizontal bore magnet and were anesthetized with 1.5% isoflurane in a 1:2 mixture of O_2/N_2O administered with a facemask (flow rate, 0.7 L/min). The mouse body temperature was maintained at 37 ± 1°C using a warm airflow and monitored with a rectal probe. Magnetic resonance imaging (MRI) experiments were done on a Bruker DBX 47/30 spectrometer (Bruker Medical) at 4.7 T equipped with a self-shielded 20 cm bore gradient system as described previously.

For determination of tumor vascular permeability and extravasion (tumor cell extracellular leakage space), the contrast agent GdDOTA (Dotarem) was injected as an intravenous bolus (30 μL); for tumor relative blood volume, the iron oxide particle (Endorem) was injected 15 min later. The principles behind measurement of these variables have already been described (26, 27). In addition, in both mice and rats, the contrast agent Vistarem was used to determine K^{trans}, extracellular leakage space (Ve), and absolute blood volume (Vp) as described previously (28).

Tumor interstitial fluid pressure. The interstitial fluid pressure (IFP) of BN472 tumors was measured as described previously (25) using the WIN method in rats anesthetized with 2.5% isoflurane delivered at 2 L/min. IFP was measured at baseline (day 0) and then twice per week for up to 2 weeks following treatment with vehicle or RAD001 (5 mg/kg three times per week orally).

Data analysis. Results are presented as mean ± 1 SE. Differences between groups was tested using a *t* test (two groups), one-way ANOVA with Dunnett's or Tukey's test, or two-way ANOVA with Tukey's test for post hoc comparisons. Where necessary, the data were normalized by taking $\log_{10}$ before statistical analyses. For all tests, the level of significance was set at $P < 0.05$ (two-tailed). Statistical calculations were done using SigmaStat 2.0 (Jandel Scientific). For comparisons of effects on SMA, a χ^2 test was used. For MRI and IFP analyses, a two-way repeated-measures ANOVA was done as well as a two-tailed *t* test to compare the changes in each variable between animals treated with vehicle or RAD001. The effect of a compound on a particular variable (e.g., tumor volume or IFP) is summarized as the T/C (mean change compared with baseline for drug-treated animals divided by the mean change in treatment for vehicle-treated animals) to provide a T/C_{IVol}, or T/C_{IFP} etc.

Results

***Pharmacokinetics and antiproliferative effects of RAD001 on tumor cell lines* in vitro *and* in vivo.** Proliferation assays done on a panel of mostly human tumor cell lines (n = 17) *in vitro* derived from breast, cervical, colon, fibrosarcoma, glioma, lung, melanoma, and renal tumors revealed a very broad range of IC_{50} values ranging from <1 nmol/L (very sensitive) to >1 μmol/L (insensitive) with median of 5 nmol/L and 25th and 75th percentiles of 2 and 797 nmol/L, respectively, and no obvious preference for histotype (Fig. 1A). Investigation of downstream signaling components of the mTOR pathway

showed similar effects in both sensitive and insensitive cell lines. Thus, in both the sensitive murine B16/BL6 melanoma (IC_{50}, 0.7 nmol/L) and the insensitive human cervical KB-31 (IC_{50}, 1,778 nmol/L), antiproliferative concentrations of RAD001 resulted in total dephosphorylation of S6K1 and the substrate S6 and a shift in the mobility of 4E-BP1, which is indicative of a reduced phosphorylation status (Supplementary Fig. S1). Interestingly, these IC_{50} values did not predict for antitumor activity *in vivo* as assessed by the maximal T/C_{IVol} determined after at least 2 weeks daily treatment with an optimal RAD001 dose (1-10 mg/kg; $r^2 = 0.06$; $P = 0.34$; $n = 17$; see Fig. 1A). Thus, significant antitumor activity *in vivo* ($T/C_{IVol} < 0.4$) was observed in tumors derived from four insensitive tumors with IC_{50} values > 1 μmol/L, whereas tumors derived from sensitive cell lines *in vitro* (IC_{50} < 10 nmol/L) showed a variable antitumor response *in vivo*: T/C_{IVol} ranging from -0.35 to 0.7. Furthermore, antitumor activity against tumors derived from the four insensitive cell lines was observed, although plasma concentrations of RAD001 were >1 μmol/L for only ~4 h post-dosing and the maximal concentrations achieved in tumor tissue were >10-fold below the IC_{50} for inhibition of proliferation of these cells *in vitro* (Fig. 1B). These data implied that activity *in vivo* might include a nontumor cell component of the solid tumor such as various stromal cells within the vascular compartment.

Consistent with the hypothesis that the antitumor activity of RAD001 included a stromal component, Fig. 2A to D shows that the dose-dependent inhibition of solid tumor growth *in vivo* of both sensitive (B16/BL6) and insensitive (KB-31 and HCT-116) models is accompanied by marked effects on the vascular compartment after 2 to 3 weeks daily treatment (Fig. 2E and F). In all three models, RAD001 decreased the BVD at least 2-fold as determined by CD31 staining and Tie-2 content (total vessels) and by Hoechst dye (perfused vessels) even in the relatively poorly vascularized models of KB-31 and HCT-116. In the B16/BL6 model, these effects were seen in both primary (ear) tumor and lymph node metastases, and microscopy revealed that in all cases the tumor periphery had some vessels but the centre was largely necrotic (Supplementary Fig. S2). RAD001 also dose-dependently decreased the amount of metastases formed in the lung in the B16/BL6 model. At all doses and in all models, RAD001 treatment was very well tolerated with no body weight loss recorded (results not shown).

Antiangiogenic/vascular effects of RAD001* in vitro *and* in vivo *in comparison with PTK/ZK. RAD001 potently inhibited VEGF-induced HUVEC proliferation in the picomolar range and bFGF-induced proliferation in the nanomolar range but was less effective against FBS-induced proliferation (Table 1A). RAD001 had no effects on VEGF-induced HUVEC migration at concentrations up to 100 nmol/L. In contrast, the pan-VEGFR inhibitor PTK/ZK selectively inhibited VEGF-induced proliferation and migration within the same nanomolar range (IC_{50} proliferation, 12 ± 3 nmol/L; IC_{50} migration, 18 ± 6 nmol/L)

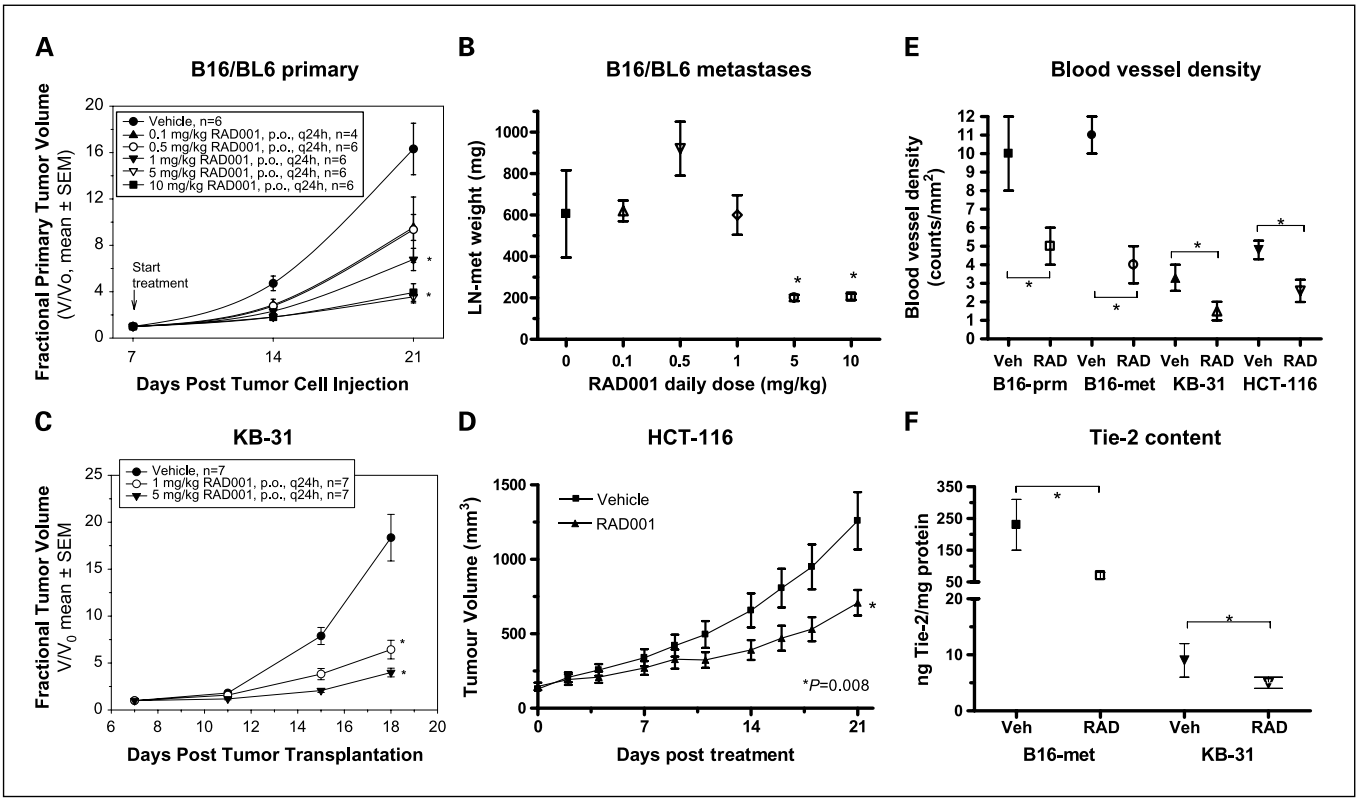

Fig. 2. Antiproliferative/antivascular activity of RAD001 in sensitive and insensitive solid tumor models. Tumor models of murine B16/BL6 melanoma (*A* and *B*) and human tumor xenografts KB-31 (*C*) and HCT-116 (*D*) were set up as described in Materials and Methods. Antiproliferative effects are shown as the tumor volume or metastasis weight after daily oral treatment with 0.1 to 10 mg/kg RAD001 (B16/BL6), 5 or 10 mg/kg (KB-31), or 10 mg/kg (HCT-116). After 2 to 3 wk of treatment, mice were perfused for 60 s with Hoechst 33342 and sacrificed and the tumors were ablated. Tumors slices (10 μm) were prepared for examination by microscopy at a magnification of 200-fold or tumors were homogenized and Tie-2 quantified by ELISA (Materials and Methods). Mean ± SE for the highest doses used. *, $P < 0.05$, versus the respective vehicle using a two-tailed *t* test or one-way ANOVA as appropriate.

Table 1. Differential antiangiogenic/antivascular effects of RAD001 and PTK/ZK *in vitro* and *in vivo*

(A) Effects on cell proliferation and migration *in vitro*

***In vitro* assay**	**IC_{50}, nmol/L (mean ± SE)**	
	RAD001	**PTK/ZK**
HUVEC proliferation + VEGF	0.12 ± 0.22	12 ± 3
HUVEC proliferation + bFGF	0.8 ± 0.4	6,600, >1,000
HUVEC proliferation + FBS	>10	1,700, >1,000
HUVEC migration + VEGF	>100	18 ± 6
Normal human dermal fibroblast proliferation + VEGF	>10	7,640 ± 2,742

(B) Effects of RAD001 on VEGF production *in vitro*

Tumor cell line and culture conditions	**VEGF concentration in supernatant (pg/10^5 cells)**			
	RAD001 concentration in medium (nmol/L)			
	0	**2**	**20**	**200**
KB-31 + 10% FBS	90 ± 10	70 ± 2*	63 ± 1*	62 ± 1*
KB-31 + 0.5% FBS	60 ± 5	58 ± 1*	58 ± 2*	40 ± 1*
	0	**0.02**	**0.2**	**2**
B16/BL6 + 10% FBS	400 ± 20	390 ± 10	320 ± 2*	120 ± 2*
B16/BL6 + 0.5% FBS	420 ± 10	425 ± 5	280 ± 5*	80 ± 2*

(C) Effects in growth factor implant angiogenesis (chamber) model

Growth factor used and variable measured	**Daily dose of compound (mg/kg)**						
	RAD001					**PTK/ZK**	
	0	**0.1**	**1**	**5**	**10**	**0**	**100**
	Total quantity in vascularized tissue (μL blood or ng Tie-2)						
Total blood + VEGF	68 ± 8	94 ± 12	90 ± 10	96 ± 11	106 ± 10†	81 ± 14	38 ± 7†
Total blood + bFGF	61 ± 8	98 ± 17	137 ± 17†	—	166 ± 18†	131 ± 30	48 ± 11†
Total Tie-2 + VEGF	145 ± 16	163 ± 20	96 ± 12†	75 ± 9†	61 ± 8*	130 ± 16	66 ± 9†
Total Tie-2 + bFGF	129 ± 16	173 ± 22	188 ± 32	—	103 ± 20	232 ± 35	100 ± 15†

(D) Effects on dye extravasation *in vivo*

Vessel permeability	**Treatment (mg/kg)**		
	Vehicle	**RAD001 (5)**	**PTK/ZK (50)**
	Evans blue dye area (mm^2)		
-VEGF	13 ± 2	20 ± 6	4 ± 3‡
+VEGF	28 ± 6	35 ± 9	10 ± 3§

NOTE: *In vitro.* (A) Cells were seeded at a density of 5×10^3 per well. IC_{50} values: After 24 h, growth medium was replaced by basal medium containing 1.5% FBS. After another 24 h, the medium was replaced by basal medium containing 5% FBS, VEGF (10 ng/mL), or bFGF (0.5 ng/mL) with or without RAD001. After 24 h incubation, bromodeoxyuridine labeling solution was added and cells were incubated a further 24 h before fixation, blocking, and addition of peroxidase-labeled anti-bromodeoxyuridine antibody. Bound antibody was detected colorimetrically at 450 nm using tetramethylbenzidine. Mean ± SE for the IC_{50} of at least three determinations or the values in each experiment. (B) VEGF: B16/BL6 or KB-31 cells were incubated with 10% FBS for 24 h and then treated with increasing concentrations of RAD001 in medium containing 10% (growing cells) or 0.5% FBS (nongrowing cells). VEGF concentrations were measured by ELISA. Simultaneous quantification of the number of viable cells was done to allow correction of VEGF levels for cell number.
In vivo. (C) Growth factor implant angiogenesis (chamber) model: Porous chambers containing VEGF (2 μg/chamber) or bFGF (0.3 μg/chamber) in 0.5 mL of 0.8% (w/v) agar (containing 20 units heparin/mL) were implanted subcutaneously in the flank of mice. Growth was quantified by measuring the weight (tissue formation), hemoglobin converted to unit of blood (number of vessels and also bleeding), and Tie-2 (number of endothelial cells, vessel density) content of the tissue. Mice were treated orally once daily with PTK/ZK (100 mg/kg), RAD001 (0.1, 0.5, 1, 5, and 10 mg/kg), or vehicle starting 4 to 6 h before implantation of the chambers and continuing for 4 d. The animals were sacrificed for measurement of the vascularized tissues 24 h after the last dose. Mean ± SE. (D) Evans blue extravasation: VEGF-coated beads were implanted intradermally in the ears of C57/BL6 mice. After 2 d, mice were treated once with the doses of RAD001 or PTK/ZK shown, and after 2 h, permeability was assessed by measurement of the area and intensity of Evans blue dye leaking into the tissue 5 min after intravenous injection. Mean ± SE (n = 8).
*$P < 0.05$, statistical significance of change compared with vehicle-control (one-way ANOVA).
†$P < 0.05$, statistical significance of change compared with control with growth factor alone (ANOVA n = 6 per group per experiment and two pooled experiments).
‡$P < 0.05$, statistical significance of change compared with vehicle (one-way ANOVA).
§$P < 0.001$, statistical significance of change compared with vehicle (one-way ANOVA).

but displayed no effect on bFGF- or FBS-induced proliferation at concentrations exceeding 1 μmol/L. Neither RAD001 nor PTK/ZK had significant effects on bFGF-mediated proliferation of normal human dermal fibroblasts, indicating a specificity for endothelial cells of >10-fold (Table 1A), especially when VEGF-stimulated. Culture of KB-31 and B16/BL6 cell lines using serum-replete (10% FBS) or serum-deprived (0.5% FBS) conditions showed that, under both conditions, RAD001 significantly inhibited VEGF production in the sensitive B16/BL6 (≥0.2 nmol/L) and insensitive (≥2 nmol/L) cell lines at concentrations achievable *in vivo* (Table 1B). Note the 4- to 7-fold lower VEGF levels in KB-31 cells compared with B16/BL6 cells consistent with the lower vascularization of the solid KB-31 tumor observed *in vivo* (Fig. 2E and F; Supplementary Fig. S2).

Further comparisons of RAD001 and PTK/ZK were made *in vivo* using a chamber impregnated with growth factor (VEGF or bFGF) implanted subcutaneously in a mouse and treated for 4 days with RAD001 or PTK/ZK. The effect of RAD001 treatment (0.1-10 mg/kg/d) was selective and differed from the effects of PTK/ZK (100 mg/kg; see Table 1C). With either growth factor, RAD001 dose-dependently increased the hemoglobin content (converted to blood equivalents and indicative of the number of vessels as well as vascular leakiness) but reduced the Tie-2 content (number of endothelial cells indicative of the number of vessels) and this was significant for VEGF stimulation but not bFGF stimulation. In contrast, PTK/ZK significantly reduced total hemoglobin and Tie-2 content in the presence of either growth factor (Table 1C). Thus, although RAD001 did not inhibit tissue formation, it did specifically inhibit VEGF-induced new vessel formation and actually tended to increase VEGF-induced vessel leakiness, the opposite effect of PTK/ZK.

Effects on VEGF-induced vessel leakiness were also investigated using a modified Miles assay where the amount of dye extravasated after implantation of VEGF-coated beads in mouse skin was measured. PTK/ZK significantly reduced vascular leakiness with or without the administration of exogenous VEGF (Table 1D). In contrast, RAD001 did not reduce leakiness but again tended to increase it ($P = 0.06$ in the presence of VEGF; see also Supplementary Fig. S3).

Antiangiogenic/vascular effects of RAD001 in comparison with PTK/ZK in the B16/BL6 tumor model. As already described (Fig. 2A and B), daily treatment with RAD001 dose-dependently inhibited growth of the primary (ear) and lymph node metastases of B16/BL6 melanoma, and PTK/ZK (100 mg/kg/d orally for 2 weeks) was also efficacious: $T/C_{TVol} = 0.5$ and 0.3 on the primary and lymph node metastases respectively (data not shown). At the endpoint (2 weeks treatment), VEGF levels were measured in the plasma and also in the lymph node metastases in the same experiments where effects on the vasculature were examined by immunohistochemistry. Both compounds significantly reduced total levels of VEGF in the plasma, but only RAD001 had a significant effect on the lymph node metastases (Fig. 3A). When VEGF levels were expressed as concentration in the lymph node metastases (Fig. 3B), neither compound had an effect and PTK/ZK actually tended to increase the concentration. Plasma VEGF levels significantly correlated ($P < 0.0001$) with the size of the lymph node metastases (Fig. 3C). Histologic examination of the lymph node metastases also showed a difference in effects on SMA staining (Fig. 3D and E), which is a marker of the smooth muscle cells or pericytes that cover and stabilize blood vessels and are an indication of the maturity of blood vessels. In tumors derived from vehicle-treated animals, ~40% of the vessels had an intact pericyte layer (Fig. 3D, *middle*), whether partial or completely SMA-covered; thus, 60% vessels had no coverage at all (Fig. 3E). RAD001 decreased the total number of vessels (Fig. 3D) and very strongly reduced the mature vessels with SMA staining (Fig. 3D), an effect limited to those vessels with complete coverage (Fig. 3E). PTK/ZK also significantly reduced the total number of vessels but had much less effect on vessels with an intact SMA staining (Fig. 3D).

Dynamic contrast-enhanced MRI (DCE-MRI) was used to image vascular effects noninvasively. Despite significant antitumor efficacy against the B16/BL6 lymph node metastases (Fig. 4A), RAD001 failed to affect tumor blood vessel permeability (Fig. 4B) as measured by the vascular transfer constant K^{trans}. Indeed, as in the VEGF-induced vascular leakage models, there was a trend for an increase in comparison with vehicle-treated mice: $T/C_{K^{trans}} = 1.3$ and 1.4 on days 3 and 7, respectively (see also Table 2). In both vehicle and RAD-treated groups, the tumor blood volume (Vp) tended to decrease, but there was no difference between the treated-groups (Fig. 4C): $T/C_{Vp} = 0.95$ and 0.70 on days 3 and 7, respectively (Table 2). However, RAD001 significantly decreased the extracellular space (Ve) compared with baseline ($P = 0.03$) after 7 days and this was close to significance ($P = 0.07$) compared with vehicle ($T/C_{Ve} = 0.7$; see Fig. 4D). The absence of an effect on vascular permeability or K^{trans} was reproducible in the B16/BL6 lymph node metastases and also in another syngeneic model of rat mammary BN472 tumors implanted in the breast (Table 2; Supplementary Fig. S4A and B), which was in contrast to the effects already reported for PTK/ZK (26, 28). In neither model was there a significant correlation between any of the basal DCE-MRI variables and the eventual tumor response on day 6 or 7 (T/C_{TVol}), although in both tumor types there was a trend for a larger initial blood volume to be associated with a better tumor response. BN472 tumors are also well-vascularized; despite relatively low sensitivity to rapid antiproliferative effects of RAD001, longer treatment (14 days) led to significant inhibition of growth ($T/C_{TVol} = 0.26$, 0.43, and 0.56 in three independent experiments) and this was associated with a significant decrease in tumor IFP of ~30% after ≥7 days treatment in two independent experiments (results not shown).

Discussion

Seventeen different tumor cell lines were screened for their *in vitro* sensitivity to RAD001 and this revealed a broad range of sensitivities, from 0.7 nmol/L (B16/BL6) to 4 μmol/L (HCT-116), apparently with some cells displaying innate resistance toward mTOR pathway inhibition (e.g., HCT-116 and KB-31) despite significant downstream effects on the pS6 and 4E-BP1 pathways. Exactly which molecular determinants predict responsiveness of tumor cells to RAD001 is still unclear but may include c-myc overexpression (29), inability to regulate p27 levels in response to treatment (30), levels and activity of cyclin D (31), Bcl-2, and CDK4 (32), deregulation of eIF-4E, and potentially mutations in pS6 kinase or mTOR (33). Our data, discussed below, suggest that, *in vivo*, other important

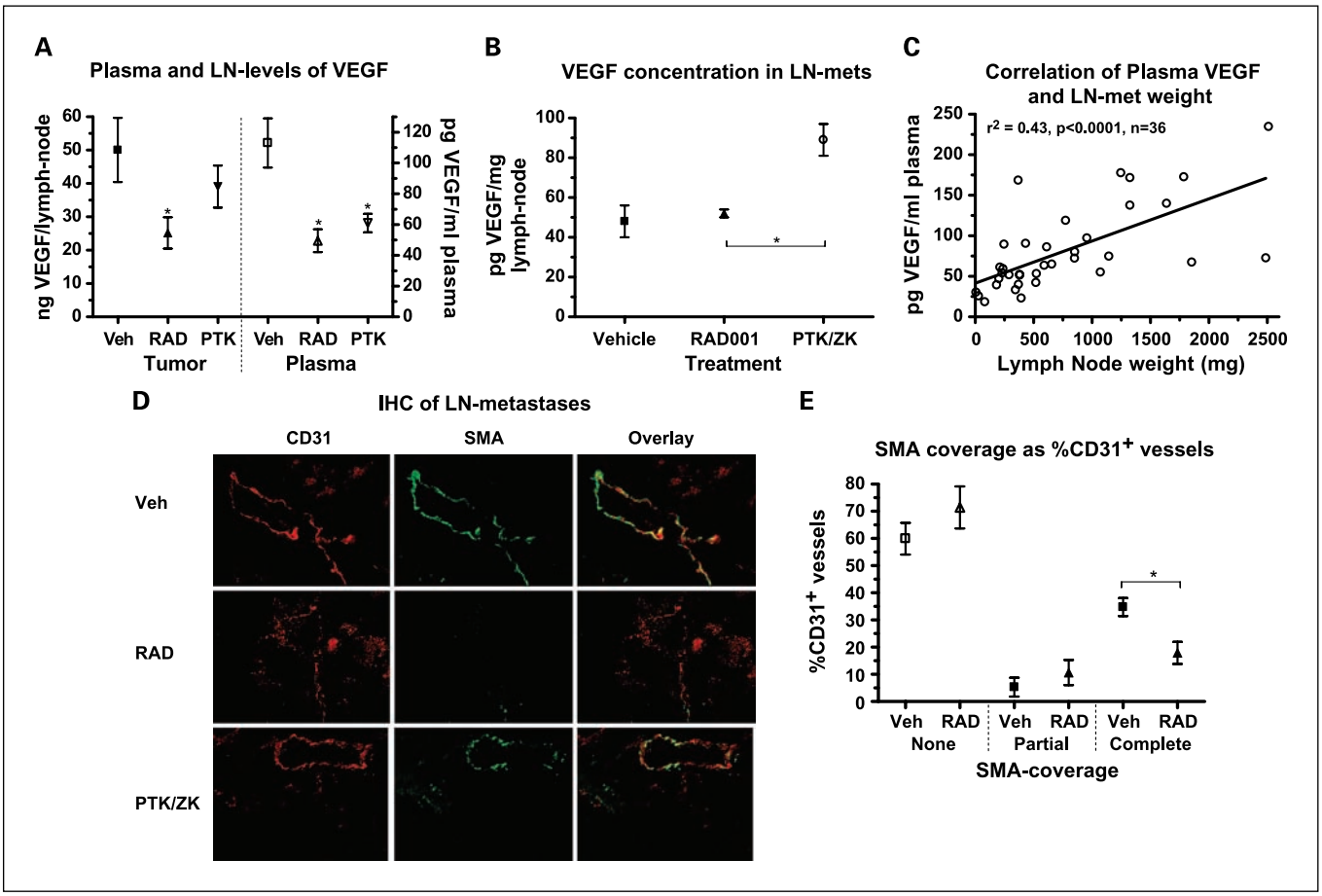

Fig. 3. Comparison of effects of RAD001 and PTK/ZK in the B16/BL6 model *in vivo*. B16/BL6 melanoma tumor cells were injected intradermally in the ear of C57/BL6 mice and after 7 d treated with RAD001 (5 mg/kg orally), vehicle control, or PTK/ZK (100 mg/kg) once daily for 2 more weeks. At day 21, mice were sacrificed and tumors were excised, weighed, and frozen in OCT in isopentane in a dry ice bath. Cryosections of 10 μm were directly mounted and photographed directly or stained for CD31 (marker of endothelial cells) and SMA (a marker for smooth muscle cells). Murine VEGF levels were determined by ELISA. Total amounts were estimated using the determined concentration multiplied by the total lymph node (*LN*) weight. Mean ± SE (n = 6-12). *, $P < 0.05$, significant inhibition compared with vehicle control using a one-way ANOVA (*A* and *B*) or χ^2 test (*E*).

factors influence tumor sensitivity to RAD001, which can be broadly described as antiangiogenic and antivascular.

The pharmacokinetics of RAD001 in mice showed that maximum levels of only 0.1 μmol/L are achieved in a human tumor xenograft following a single administration, whereas plasma levels reach 1 to 3 μmol/L for ~4 h. Thus, in principle, tumor levels of RAD001 would be insufficient to inhibit cell proliferation in the insensitive tumors such as HCT-116 and KB-31, yet inhibition of growth of these tumors was shown after 1 to 3 weeks of treatment. Indeed, there was only a very weak, nonsignificant correlation between the IC_{50} (*in vitro*) and the activity *in vivo* (T/C_{TVol}) for 17 different cell lines. Although this discrepancy could be explained by (*a*) the relatively artificial assay format of cells growing in monolayers and (*b*) the altered sensitivity of cells growing *in vivo* through the presence of different concentrations of growth factors, the data suggested that there could also be an important direct activity against nontumor cells (stromal cells in the solid tumor such as fibroblasts, pericytes, and endothelial cells) because mTOR is ubiquitously expressed. Furthermore, downstream effects on pS6 and 4E-BP1, and thus translation of proteins that are known to include HIF-1 (1), would lead to a reduction of VEGF levels, which is an important survival factor for endothelial cells (7, 34). Here, we did not show an effect on HIF-1, although others have done so for RAD001 (14) and the rapamycin prodrug temsirolimus (21, 22), but we did show significant pathway inhibition and decreases in VEGF production in both sensitive and insensitive cell lines both in cell culture and when grown as solid tumors. Moreover, in the *in vivo* models, RAD001 significantly reduced circulating VEGF levels and there was no reactive increase in VEGF in the tumor tissue as was observed after selective VEGF inhibition with PTK/ZK.

In support of an effect on stromal cells and maybe also as a consequence of effects on HIF-1 and VEGF, RAD001 decreased Tie-2 levels in a mouse chamber model after 4 days of treatment. After 2 to 3 weeks of treatment, a reduction in Tie-2 was also observed in tumor xenografts derived from both sensitive and insensitive cell lines as well as a significant reduction in tumor BVD as indicated by both reduction of CD31 staining (a marker of endothelial cell number) and Hoechst dye staining (a marker for the number of patent blood vessels). Although a reduction in BVD does not prove a direct effect on the vasculature after such prolonged treatment, it is consistent with the hypothesis, and the 2-fold decrease in BVD observed in comparison with vehicle controls may actually underestimate the effect because untreated tumors tend to

outgrow their blood supply (35) and show increased hypoxia (36). Furthermore, *in vitro*, RAD001 showed potent activity against VEGF-induced proliferation of HUVECs with IC_{50} values in the subnanomolar range, and at higher concentrations also against bFGF-induced HUVEC proliferation, but showed 10- to 100-fold less activity against fibroblasts. RAD001 has also been shown to potently inhibit growth factor-driven cell proliferation *in vitro* of bovine vascular smooth muscle cells (37). All of these data show that an important antiangiogenic/vascular component exists for RAD001, which may be the major mechanism of action of RAD001 against tumors with innate insensitivity to mTOR inhibition.

Some of these *in vitro* and *in vivo* antiangiogenic/vascular effects were similar to those described for the pan-VEGFR inhibitor, PTK/ZK, but interestingly, others were different. Thus, although PTK/ZK also inhibited VEGF-stimulated HUVEC proliferation, it had no effect when the cells were stimulated by bFGF or FBS. *In vitro*, PTK/ZK inhibited HUVEC migration, but RAD001 was without effect. In addition, in a growth factor implant angiogenesis model, PTK/ZK reduced vascularization (Tie-2 content) independent of the type of growth factor used and reduced total blood content, whereas RAD001 tended to increase vascular leakiness. Differential effects on normal tissue permeability were confirmed in a second model using a modified Miles assay. Thus, the two compounds tended to have opposite effects on tissue permeability. In the B16/BL6 tumor model, PTK/ZK and RAD001 both reduced BVD, but RAD001 was much more effective at reducing the mature vessels with SMA coverage. A minimal or absence of an effect by PTK/ZK on mature (SMA)-covered blood vessels has also been reported in other models (38). Both compounds reduced circulating VEGF concentrations possibly as a reflection of their effect on tumor size and RAD001 also reduced total tumor VEGF. However, neither compound significantly reduced VEGF concentrations in tumor tissue, and PTK/ZK actually increased it compared with RAD001. These data suggest that a feedback mechanism may operate to increase VEGF production in response to inhibition of the VEGF signaling pathway and this feedback may be less acute after mTOR inhibition. Changes in plasma VEGF cannot distinguish between a blockade of VEGF production by the tumor, as we have shown *in vitro*, and a reduction in the tumor tissue, which is the source of VEGF, or a combination of both, but the data suggest that plasma VEGF may be a useful marker of efficacy as recently described for the VEGF antibody bevacizumab (39).

Finally, in confirmation of the two models measuring VEGF-induced tissue leakiness, RAD001 failed to decrease tumor vascular permeability or K^{trans} in two different well-vascularized

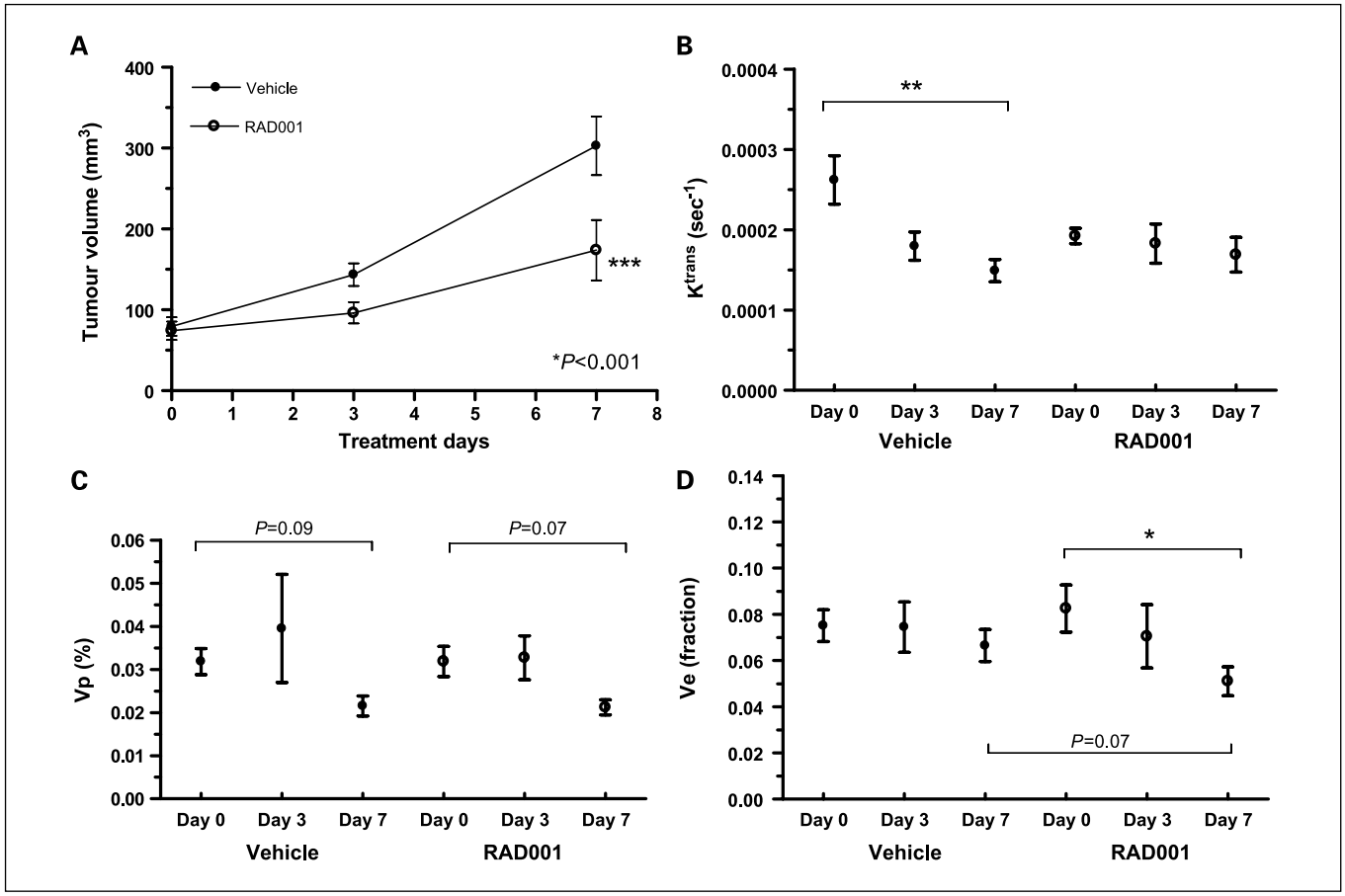

Fig. 4. Effects of RAD001 on MRI measured variables in B16/BL6 lymph node metastases. B16/BL6 melanoma tumor cells were implanted intradermally in the ear of C57/BL6 mice and after 14 d (baseline; day 0) were treated with RAD001 (10 mg/kg orally) or vehicle daily for 7 d. The contrast agent Vistarem was injected as an intravenous bolus on day 0 (before treatment) and days 3 and 7 post-treatment to determine tumor vessel transfer coefficient (K^{trans}), extracellular leakage space (Ve), or blood volume (Vp). Mean ± SE from paired mice (n = 16 for vehicle and n = 14 mice for RAD001). *, $P < 0.05$; **, $P < 0.01$, (two-way repeated-measures ANOVA); ***, $P < 0.001$ (two-tailed t test).

Table 2. Summary of effects of RAD001 on DCE-MRI models

	Tumor model	Time point (d)	T/C ratio			
			ΔTVol	VP	LS	rBVol
E1	Murine B16 lymph node metastases	2	0.37*	1.26	1.03	0.88
			ΔTVol	K^{trans}	Ve	Vp
E2	Murine B16 lymph node metastases	3	0.42*	1.31	0.95	0.95
		7	0.28 †	1.39	0.70 ‡	0.70
E3	Rat BN472	2	0.28	0.76	0.97	0.71
		6	0.63	0.81	1.23	0.90

NOTE: Summary of data from three different series of DCE-MRI experiments using either murine B16/BL6 melanoma lymph node metastases or rat mammary BN472 orthotopic tumors (Materials and Methods). Results show the T/C ratio for the different variables shown from $n = 9$ and 10 mice in experiment 1 (E1), $n = 16$ and 14 mice in experiment 2 (E2), and $n = 6$ and 6 mice in experiment 3 (E3) for vehicle and RAD-treated mice, respectively. In experiment 1, the contrast agent GdDOTA was used to determine tumor vascular permeability (VP), extracellular leakage space (LS), or relative blood volume (rBVol). In experiments 2 and 3, the contrast agent Vistarem was used to determine tumor vessel transfer coefficient (K^{trans}), extracellular leakage space (Ve), or blood volume (Vp). Full experimental results are shown in Supplementary Fig. S4.
*$P = 0.02$ (two-tailed t test).
†$P < 0.001$ (two-tailed t test).
‡$P = 0.07$ (two-tailed t test).

tumor models (B16/BL6 model and BN472) as measured noninvasively by DCE-MRI. This variable is considered the classic marker of an antiangiogenic agent targeting the VEGFR signaling system, and decreases in various experimental tumor models have been described for PTK/ZK (26, 28, 40), sunitinib (41), or bevacizumab (42). In fact, consistent with the observations on VEGF-induced tissue leakiness in C57/BL6 mice, RAD001 tended to increase permeability in B16/BL6 tumors grown in these mice, although there was a trend for a decrease in the BN472 model in K^{trans}. The lack of blockade by RAD001 of VEGF-induced vascular leakiness may be due to (*a*) the pronounced effect of RAD001 on the protective pericyte coverage on vessels allowing leakage of blood into surrounding tissue and/or (*b*) the well-recognized negative feedback loop of S6K down-regulation leading to increased activation of phospho-Akt, which activates endothelial nitric oxide synthase (28).

The DCE-MRI also showed that there was no consistent effect on extracellular (leakage) space, whereas, overall across all models, there was a trend for RAD001 to slightly reduce tumor blood volume after 2 to 7 days of treatment. One would expect tumor blood volume to reflect BVD, which was reduced by RAD001 after 2 to 3 weeks of treatment and it may be the different timescales and/or possibility that pools of blood exist in solid tumors, which explains this apparent discrepancy. Alternatively, because RAD001 apparently tended to increase vascular leakiness by destroying the pericyte coverage, this may lead to an increase in tumor blood volume, which is eventually counteracted by a decrease in the number of viable blood vessels after longer treatment. In the BN472 tumor model, IFP has been shown to strongly correlate with tumor blood volume (25); indeed, RAD001 was only able to reduce the IFP of BN472 after at least 1 week of treatment, which also suggests that longer treatment may be necessary to significantly reduce the tumor vasculature.

Thus, in conclusion, our data suggest that the antitumor activity of RAD001 in solid tumors exhibits a strong antivascular and antiangiogenic component, which, however, differs in several ways from agents targeting the VEGFR signaling pathway. The most important difference may prove to be the increased activity against the more mature vasculature of tumors, which by implication includes the tumor pericytes. This is because effects on VEGF inhibition have been shown to be incomplete and impermanent; inhibition by VEGFR inhibitors followed by cessation leads to the persistence of the basement membrane and pericytes allowing rapid recovery of the vasculature (38, 43). Consequently, due to a more complete inhibition of tumor vascularization directly (endothelial and smooth muscle cells and pericytes) and indirectly (via VEGF), RAD001 may be expected to be an effective therapy in combination with targeted inhibitors of VEGF signaling or indeed as monotherapy before or after VEGFR inhibitors. Consistent with this hypothesis, RAD001 has recently been shown to double progression-free survival in patients with kidney cancer, which were refractory to treatment with the multikinase inhibitors sunitinib or sorafenib (44).

Disclosure of Potential Conflicts of Interest

No potential conflicts of interest were disclosed.

Acknowledgments

We thank the following for excellent technical assistance in all the methods described herein: Mike Becquet, Stephane Ferretti, Jose Figueiredo, Marc Hattenberger, Matthieu Klopfenstein, Marina Maurer, Melanie Muller, Hans-Peter Mueller, Beatrice Probst, Fabienne Schaeffer, Andy Theuer, and Julianne Vaxelaire.

References

1. Bjornsti M-A, Houghton PJ. The TOR pathway: a target for cancer chemotherapy. Nat Rev Cancer 2004;4:335–48.
2. Boulay A, Lane HA. The mammalian target of rapamycin kinase and tumor growth inhibition. Recent Results Cancer Res 2007;172:99–124.
3. Fingar DC, Blenis J. Target of rapamycin (TOR): an integrator of nutrient and growth factor signals and coordinator of cell growth and cell cycle progression. Oncogene 2004;23:3151–71.
4. Albanell J, Dalmases A, Rovira A, Rojo F. mTOR signalling in human cancer. Clin Transl Oncol 2007;9:484–93.

5. Guertin DA, Sabatini DM. Defining the role of mTOR in cancer. Cancer Cell 2007;12:9–22.
6. Sarbassov DD, Ali SM, Kim D-H, et al. Rictor, a novel binding partner of mTOR, defines a rapamycin-insensitive and raptor-independent pathway that regulates the cytoskeleton. Curr Biol 2004;14:1296–302.
7. Folkman J. Angiogenesis in cancer, vascular, rheumatoid and other disease. Nat Med 1995;1:27–31.
8. Li DF, Hung MC. All roads lead to mTOR: integrating inflammation and tumor angiogenesis. Cell Cycle 2007;6:3011–14.
9. Jung BH, Liu LZ. PI3K/PTEN signaling in tumorigenesis and angiogenesis. Biochim Biophys Acta 2008; 1784:150–58.
10. Humar R, Kiefer FN, Berns H, et al. Hypoxia enhances vascular cell proliferation and angiogenesis *in vitro* via rapamycin (mTOR)-dependent signaling. FASEB J 2002;16:771–80.
11. Francesc V, Chambard JC, Pouysségur J. p70 S6 kinase-mediated protein synthesis is a critical step for vascular endothelial cell proliferation. J Biol Chem 1999;274:26776–82.
12. Yu Y, Sato JD. MAP kinases, phosphatidylinositol 3-kinase, and p70 S6 kinase mediate the mitogenic response of human endothelial cells to vascular endothelial growth factor. J Cell Physiol 1999;178: 235–46.
13. Dormond O, Madsen JC, Briscoe DM. The effects of mTOR-Akt interactions on anti-apoptotic signalling in vascular endothelial cells. J Biol Chem 2007;282: 23679–86.
14. Mabuchi S, Altomare DA, Cheung, et al. RAD001 inhibits human ovarian cancer cell proliferation, enhances cisplatin-induced apoptosis, and prolongs survival in an ovarian cancer model. Clin Cancer Res 2007;13: 4261–70.
15. Mabuchi S, Altomare DA, Connolly DC, et al. RAD001 (everolimus) delays tumor onset and progression in a transgenic mouse model of ovarian cancer. Cancer Res 2007;67:2408–13.
16. Manegold PC, Paringer C, Kulka U, et al. Antiangiogenic therapy with mammalian target of rapamycin inhibitor RAD001 (everolimus) increases radiosensitivity in solid cancer. Clin Cancer Res 2008;14:892–900.
17. Shinohara ET, Cao C, Niermann K, et al. Enhanced radiation damage of tumor vasculature by mTOR inhibitors. Oncogene 2005;24:5414–22.
18. Guba M, Koehl GE, Neppl, et al. Dosing of rapamycin is critical to achieve an optimal antiangiogenic effect against cancer. Transplant Int 2005;18:89–94.
19. Semela D, Piguet A-C, Kolev M, et al. Vascular remodeling and antitumoral effects of mTOR inhibition in a rat model of hepatocellular carcinoma. J Hepatol 2007;46:840–48.
20. Phung TL, Ziv K, Dabydeen D, et al. Pathological angiogenesis is induced by sustained Akt signalling and inhibited by rapamycin. Cancer Cell 2006;10:159–70.
21. Del Bufalo D, Ciuffreda L, Trisciuoglio D, et al. Antiangiogenic potential of the mammalian target of rapamycin inhibitor temsirolimus. Cancer Res 2006;66: 5549–54.
22. Wan X, Shen N, Mendoza A, Khanna C, Helman LJ. CCI-779 inhibits rhabdomyosarcoma xenograft growth by an antiangiogenic mechanism linked to the targeting of mTOR/Hif-1α/VEGF signaling. Neoplasia 2006;8:394–401.
23. Wood JM, Bold G, Buchdunger E, et al. PTK787/ZK 222584, a novel and potent inhibitor of vascular endothelial growth factor receptor tyrosine kinases, impairs vascular endothelial growth factor-induced responses and tumor growth after oral administration. Cancer Res 2000;60:2178–89.
24. Sini P, Samarzija I, Baffert F, et al. Inhibition of multiple vascular endothelial growth factor receptors (VEGFR) blocks lymph node metastases but inhibition of VEGFR-2 is sufficient to sensitize tumor cells to platinum-based chemotherapeutics. Cancer Res 2008; 68:1581–92.
25. Ferretti S, Allegrini P, O'Reilly T, et al. Patupilone induced vascular disruption in orthotopic rodent tumor models detected by magnetic resonance imaging and interstitial fluid pressure. Clin Cancer Res 2005;11: 7773–84.
26. Rudin M, McSheehy PM, Allegrini PR, et al. PTK787/ZK222584, a tyrosine kinase inhibitor of vascular endothelial growth factor receptor, reduces uptake of the contrast agent GdDOTA by murine orthotopic B16/BL6 melanoma tumours and inhibits their growth *in vivo*. NMR Biomed 2005;18:308–21.
27. Drevs J, Muller-Driver R, Wittig C, et al. PTK787/ZK 222584, a specific vascular endothelial growth factor-receptor tyrosine kinase inhibitor, affects the anatomy of the tumor vascular bed and the functional vascular properties as detected by dynamic enhanced magnetic resonance imaging. Cancer Res 2002;62:4015–22.
28. Schnell CR, Stauffer F, Allegrini PR, et al. Effects of the dual pan-class I PI3K/mTOR inhibitor NVP-BEZ235 on the tumor vasculature: implications for clinical imaging. Cancer Res 2008;68:6598–607.
29. Hosoi H, Dilling MB, Liu LN, et al. Studies on the mechanism of resistance to rapamycin in human cancer cells. Mol Pharmacol 1998;54:815–24.
30. Luo Y, Marx SO, Kiyokawa H, Koff A, Massagué J, Marks AR. Rapamycin resistance tied to defective regulation of p27Kip1. Mol Cell Biol 1996;16:6744–51.
31. Noh WC, Mondesire WH, Peng J, et al. Determinants of rapamycin sensitivity in breast cancer cells. Clin Cancer Res 2004;10:1013–23.
32. Aguirre D, Boya P, Bellet D, et al. Bcl-2 and CCND1/CDK4 expression levels predict the cellular effects of mTOR inhibitors in human ovarian carcinoma. Apoptosis 2004;9:797–805.
33. Huang S, Houghton PJ. Mechanisms of resistance to rapamycins. Drug Resist Updat 2001;4:378–91.
34. Carmeliet P and Jain RK. Angiogenesis in cancer and other diseases. Nat Insight Vasc Biol 2000;407: 249–57.
35. O'Reilly T, Wartmann M, Brueggen J, et al. Pharmacokinetic profile of the microtubule stabilizer patupilone in tumor-bearing rodents and comparison of anti-cancer activity with other MTS *in vitro* and *in vivo*. Cancer Chemother Pharmacol 2008;62: 1045–54.
36. McSheehy PM, Robinson SP, Ojugo AS, et al. Carbogen breathing increases 5-fluorouracil uptake and cytotoxicity in hypoxic murine RIF-1 tumors: a magnetic resonance study *in vivo*. Cancer Res 1998;58: 1185–94.
37. Schuler W, Sedrani R, Cottens S, et al. SDZ RAD, a new rapamycin derivative: pharmacological properties *in vitro* and *in vivo*. Transplantation 1997;64:32–5.
38. Taron M, Ramirez, F, Salazar, M, Berdiel, M, Rosell, R. Tumor and serum predictive markers of response to bevacizumab. Eur J Cancer Suppl 2007;5:27.
39. Hlushchuk R, Riesterer O, Baum O, et al. Tumor recovery by angiogenic switch from sprouting to intussusceptive angiogenesis after treatment with PTK787/ZK222584 or ionizing radiation. Am J Pathol 2008;173:1173–85.
40. Lee L, Sharma S, Morgan B, et al. Biomarkers for assessment of pharmacologic activity for a vascular endothelial growth factor (VEGF) receptor inhibitor, PTK787/ZK 222584 (PTK/ZK): translation of biological activity in a mouse melanoma metastasis model to phase I studies in patients with advanced colorectal cancer with liver metastases. Cancer Chemother Pharmacol 2006;57:761–71.
41. Marzola P, Degrassi A, Calderan L, et al. Early antiangiogenic activity of SU11248 evaluated *in vivo* by dynamic contrast-enhanced magnetic resonance imaging in an experimental model of colon carcinoma. Clin Cancer Res 2005;11:5827–32.
42. Jordan BF, Runquist M, Raghunand N, et al. Dynamic contrast-enhanced and diffusion MRI show rapid and dramatic changes in tumor microenvironment in response to inhibition of HIF-1A using PX-478. Neoplasia 2005;7:475–85.
43. Mancuso MR, Davis R, Norberg SM, et al. Rapid vascular regrowth in tumors after reversal of VEGF inhibition. J Clin Invest 2006;116:2610–21.
44. Motzer RJ, Escudier B, Oudard S, et al. Efficacy of everolimus in advanced renal cell carcinoma: a double-blind, randomised, placebo-controlled phase III trial. Lancet 2008;372:449–56.